Article

Not peer-reviewed version

Coaxial Fibres Incorporated with Phase Change Material for Thermoregulation Applications

Nathalia Hammes *, Claver Pinheiro, Iran Rocha Segundo *, Natália Cândido Homem, M. M. Silva, Helena P. Felgueiras, Graca M.B. Soares, Elisabete Freitas, Manuel F. M. Costa, Joaquim Alexandre O. Carneiro *

Posted Date: 22 February 2024

doi: 10.20944/preprints202402.1278.v1

Keywords: Phase Change Fibres; Core-Shell Fibres; Cellulose Acetate; Polyethylene Glycol 2000; Recycled Cellulose Acetate; Cooling Technologies; Wet Spinning

 doi:10.20944/preprints202402.1278.v1

Article

Coaxial Fibres Incorporated with Phase Change Material for Thermoregulation Applications

Nathalia Hammes [1,*], Claver Pinheiro [1], Iran Rocha Segundo [1,*], Natália Cândido Homem [2,3], M. Manuela P. Silva [4], Helena P. Felgueiras [3], Graça M. B. Soares [3], Elisabete Freitas [5], Manuel F. M. Costa [6] and Joaquim Alexandre O. Carneiro [1,*]

[1] Centre of Physics of Minho and Porto Universities (CF-UM-UP), Av. da Universidade, Guimarães, 4800-058, Portugal
[2] Simoldes Plastics S.A, No. 165, Rua Comendador António da Silva Rodrigues, Oliveira de Azeméis, 3720-193, Portugal
[3] Centre for Textile Science and Technology, University of Minho (2C2T - UMinho), Av. da Universidade, Guimarães, 4800-058, Portugal
[4] Centre of Chemistry of University of Minho (CQ - UMinho), Campus de Gualtar, Braga, 4710-057, Portugal
[5] University of Minho, ARISE, Department of Civil Engineering (ISISE - UMinho), Av. da Universidade, Guimarães, 4800-058, Portugal
[6] Centre of Physics of Minho and Porto Universities (CF-UM-UP), R. da Universidade, Braga, 4710-057, Portugal
* Correspondence: b13531@uminho.pt (N.H.); iran@fisica.uminho.pt (I.R.S); carneiro@fisica.uminho.pt (J.A.O.C)

Abstract: Nowadays, the growing concern about improving thermal comfort in textiles, asphalt pavements and buildings has stimulated research into phase change materials (PCMs). However, the incorporation of PCMs directly causes mechanical impacts. Therefore, this study herein reported focuses on designing coaxial phase change fibres using commercial cellulose acetate (CA) or recycled CA obtained from cotton fabrics (CAt) as a coating and polyethylene glycol (PEG) 2000 as a core. The phase change fibres (PCF) were produced by wet spinning, varying the parameters: (i) CA concentration, molecular weight and source (virgin versus recycled); and (ii) PEG concentration and ejection. For phase change recycled fibres (PCFt), PEG concentration and ejection were varied. The fibres were assessed for their optical, chemical, thermal and mechanical properties. Bright-field microscopy images and Scanning Electron Microscopy (SEM) micrographs proved the coaxial structure. Fourier Transform Infrared spectroscopy (FTIR) confirmed the presence of PEG in the core. Thermogravimetric Analysis (TGA) proved the ability of PCFs to tolerate high temperatures. Differential Scanning Calorimetry (DSC) attested to the presence of PEG2000 peaks, since their melting points were close to those of virgin PEG2000, with a slight change in the PCFs and PCFts caused by the protective sheath of CA and CAt.

Keywords: phase change fibres; core-shell fibres; cellulose acetate; polyethylene glycol 2000; recycled cellulose acetate; cooling technologies; wet spinning

1. Introduction

Civil engineering materials, such as cement and asphalt concretes, absorb high amount of solar thermal energy in the form of heat, thus contributing to heat retention far more than the natural elements in rural landscapes [1,2]. As a result, city areas often record higher air temperatures than their rural counterparts, leading to significant consequences for the environment, economy, and society [3]. Called Urban Heat Island (UHI), this phenomenon becomes more pronounced with urbanization through the construction of asphalt pavements and built structures [4,5]. It is important to emphasize that the world's population is expected to increase at least 60% in the second half of this century and this excessive growth will aggravate the urbanization [1,6]. Thus, it is essential the thermoregulation of these structures.

 doi:10.20944/preprints202402.1278.v1

As alternative, researchers have been studying the application of Latent heat thermal energy storage (LHTS) materials or simply (PCMs) (LHTS) into Civil Engineering materials to mitigate and prevent the effects of the UHI. According to this approach, the integration of PCM is a promising solution since they have dual benefits: the ability to store and release thermal energy latently, coupled with an isothermal nature during storage, thus reducing temperature fluctuations [7,8]. However, its direct application can affect the mechanical properties of the composite material.

PCM have gained significance in thermoregulating environments since their introduction in the 1980s [9]. With their high latent heat capacity, PCMs are excellent for storing energy from cooling systems or lower night-time temperatures to be released during peak heat periods, improving thermal comfort [10]. C. Pinheiro et al. [11] adopted an approach to study PCMs and observed that they differ significantly from high albedo materials. While high-albedo materials focus on reflecting solar radiation to reduce heat gain and cooling loads [11], PCMs adopt a more dynamic strategy. They absorb excess heat during periods of high temperature (such as during the day) and release it during cooler periods (such as at night) [12]. This phase change allows PCM to store and release thermal energy efficiently. So, unlike high albedo materials that passively prevent heating by reflecting solar radiation, PCMs actively balance thermal energy, absorbing and releasing heat as needed [13]. This ability to actively adjust surface temperatures makes PCM a more versatile solution for climate control in different applications, adapting to thermal variations in the environment throughout the day.

PCMs are versatile in their applications within the civil engineering [7], encompassing areas such as air conditioning systems [14], solar energy storage [15] and broadly in the integration with various construction materials [16]. Their primary purpose in these applications is to prevent damage caused by abrupt temperature changes, thus lowering the energy per area needed for heating/cooling these materials. PCMs can be incorporated directly [17,18] or encapsulated [19,20]. S. Drissi et al. [21] carried out various studies with PCM applied directly or encapsulated and, in response, the direct application method caused PCM to leak, inhibiting water migration and interfering with the hydration process, negatively affecting the development of the material's strength [22]. Therefore, in order to achieve stable PCM incorporation, so that their phase change occurs without leakage, different methods can be used to protect and encapsulate them, such as microencapsulation by sol-gel, electrospinning [23] and wet spinning [24].

B. Ozipek et al. [25] explained that the wet spinning technique is a widely used commercial process that allows the manufacture of mono- or multi-structured fibres using polymers dissolved in solvents that are extruded through small holes, forming continuous filaments in a liquid medium (coagulation bath), i.e. as the extruded filaments pass through the coagulation bath, the polymer solidifies, resulting in the formation of fibres with uniform morphology. According to A. Rohani Shirvan et al. [26], the wet spinning technique was first used to produce rayon fibres and is considered the oldest fibre spinning process. Due to its simple configuration, the wet spinning technique [27–29] has recently attracted attention as an alternative encapsulation method that allows for the stable incorporation of PCMs. The main advantage of this technique is that it does not involve heat during production, reducing the risk of possible thermal degradation. Another point is that it can produce fibres with different diameters, shapes and cross-sectional sizes. It is also a continuous process and can produce any type of polymer, which makes it a very efficient [26]. Through wet coaxial spinning, hollow or single-core fibres can be produced for different purposes, such as electronic textiles, sensors and controlled release applications [30].

Phase change fibres (PCFs) are considered intelligent materials because, in addition to containing PCMs, PCFs react to environmental changes without any human action required. On their own, PCFs recognize changes and work to maintain the standard for which they were programmed [31]. The reproducibility and the performance of coaxial fibres will depend on the rigorous selection and maintenance of wet spinning parameters [26]. Among the different existing parameters, it is necessary to take into account the evaluation of the process parameters, from solution to production, in order to obtain fibres with a well-defined core and sheath to maximise the performance of the coaxial fibres in the final application [32].

 doi:10.20944/preprints202402.1278.v1

Although several studies are exploring potential applications for the production of PCFs, there needs to be more research in the literature on this subject to broaden the range of innovation. In a study carried out by C. Chen et al. [33] where PCFs were developed using the electrospinning technique, containing CA as the support material and PEG as the PCM, it was observed that the thermal properties of PEG were different to those of virgin PEG, due to the presence of CA. S.I. Swapnil et al. [34] studied the production of fibres, via wet spinning, consisting of CA/PEG in the same solution. As a result, they observed that the viscosity of the solutions and the dH_2O used as a coagulation bath induced a more solid structure to the fibres. While the addition of PEG to the CA solution considerably increased the mechanical properties of the fibres.

To the best of the authors' knowledge, this is one of the first research works detailing the manufacturing process of wet spinning using this specific structure of PCF (coaxial fibres with CA and specially recycled CA from cotton fabrics in the protective sheath and PEG in the core). Therefore, different manufacturing parameters were studied: i) CA concentration and molecular weight, CA source (conventional versus recycled), and ii) PEG concentration, molecular weight and ejection. These fibres were analysed under their morphological using bright-field microscopy and scanning electron microscopy (SEM), chemical (ATR-FTIR), thermal (TGA, DSC) and mechanical (dynamometer) properties and compared to their analogous uniaxial and hollow fibres.

2. Materials and Methods

2.1. Materials

The materials used in this work were i) commercial cellulose acetate (CA, Sigma-Aldrich) powder, with an acetyl content of 39.8 wt.% average Mn = 30,000 and acetyl content of 39.8 wt.% by weight, average Mn = 50,000, ii) N,N-Dimethylformamide (DMF, 99%, Sigma-Aldrich), iii) N-Methyl-2-pyrrolidone (*NMP, 99%,* Sigma-Aldrich), iv) Polyethylene glycol 2,000 $H(OCH_2CH_2)_nOH$ (PEG2000, Thermo Fisher Scientific), MP = 53-55 °C, and v) dH_2O. DMF and dH_2O were used as solvent for the CA and PEG solutions, respectively.

CA, which is an ester of cellulose acetate and the most common derivative of cellulose, was selected to be the polymeric material of the protective sheath due to its natural and non-toxic characteristics, being a polymer used to produce PCFs that result in good thermal and mechanical properties [24,35].

Among the different PCMs available on the market and in the literature, polyethene glycol (PEG), was selected for the core of PCFs, as it presents interesting properties such as chemical stability, high storage capacity, wide temperature range, low overcooling behaviour and negligible volume change during its phase change [36].

Regarding the thermal proprieties of the CA and the PEG, Figures 1 and 2 show the TGA and the DSC characterization of the virgin materials under study, respectively. Regarding TGA, studies were carried out on the loss of mass of the virgin materials in relation to the increase in temperature, where the main mass loss phase for PEG2000 starts at ≈ 350 °C and ends at ≈ 430 °C. For commercial CA and CAt, the main mass loss phase starts at ≈ 315 °C and ends at ≈ 350 °C. For the DSC, the peaks, phase change temperatures and comparison of the PCFs with the Fh were analysed. For this test, the virgin materials obtained results expected from the literature.

Preprints.org (www.preprints.org) | NOT PEER-REVIEWED | Posted: 22 February 2024 doi:10.20944/preprints202402.1278.v1

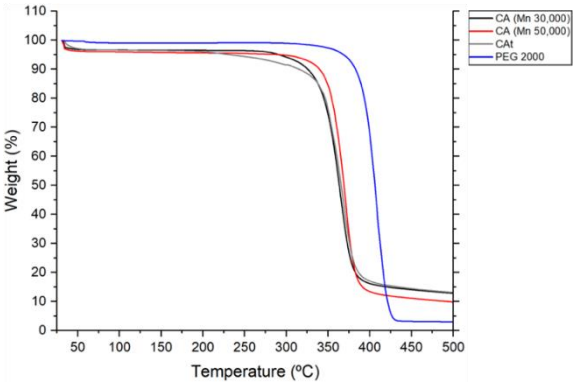

Figure 1. TGA of virgin materials, obtained from 25 to 500 °C under nitrogen atmosphere, flow rate of 200 mL/min and temperature rise of 10 °C/min.

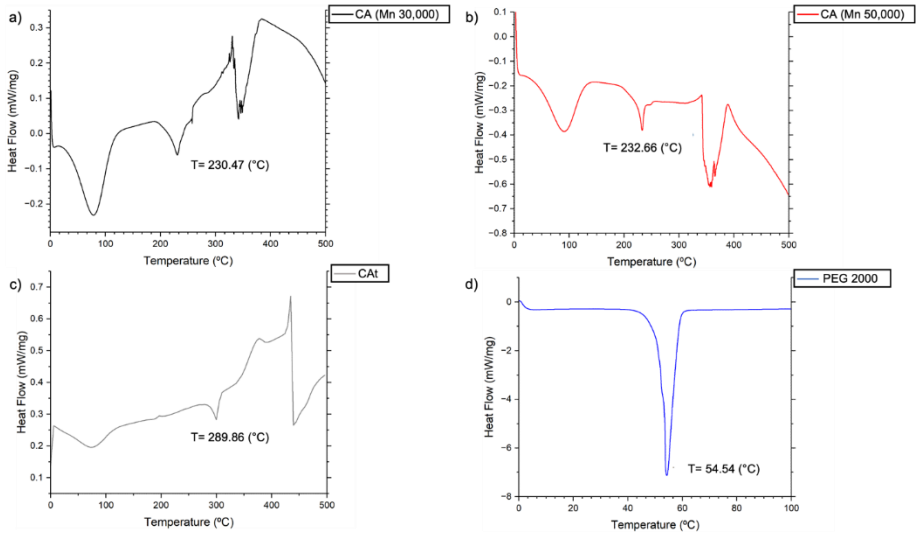

Figure 2. DSC of virgin materials. (**a**) CA (Mn 30,000). (**b**) CA (Mn 50,000). (**c**) Recycled CAt. (**d**) PEG2000.

For the synthesis of the CAt, 100% cotton fabric (from Nostrobiz, Portugal), glacial acetic acid (CH_3COOH, 100%, Pronalab), sulphuric acid (H_2SO_4, 95-98%, Sigma-Aldrich) and acetic anhydride ($(CH_3CO)2O$, 98%, AnalytiCals Carlos Erba) were used. Sodium hydroxide (NaOH, JMGS), ethanol absolute (CH_3CH_2OH, 99.5%, Merck), hydrochloric acid (HCl, 37%, Fisher Scientific), sodium hydroxide solution (NaOH, 0.25 mol/L, JMGS), hydrochloric acid solution (HCl, 0.25 mol/L, Fisher Scientific) and phenolphthalein ($C_{20}H_{14}O_4$, AnalytiCals Carlos Erba) were used to determine the degree of substitution of CAt.

2.2. Materials

As more environmentally friendly for PCFs CAt (recycled cellulose acetate from textile waste) sheath, Cat was produced using the homogeneous acetylation method [37]. In detail, 2.0 g of cotton fabric was first cut into thin strips and left in the desiccator for 24 hours. The process was started by adding 40 mL of CH_3COOH to 2.0 g of the cotton fabric. This mixture was stirred for 30 minutes at room temperature. Subsequently, a solution of H_2SO4 and CH_3COOH (0.3 mL and 17.5 mL, respectively) was added and the mixture was stirred for 15 minutes at room temperature. After 15 minutes, the textile was filtered and separated from the solution. At this point, 20 mL of $(CH_3CO)_2O$ was added to the liquid, the textile was replaced and the solution stirred at room temperature for 24 hours. After 24 hours, the solution was removed from the stirrer and slowly added to a beaker containing 1.0 L of dH_2O. Finally, the CAt was vacuum filtered (Diaphragm Vacuum Pump N810,

 doi:10.20944/preprints202402.1278.v1

LABOPORT, Germany) and washed with dH_2O until pH 7 was reached. The CAt was dried in a drying and sterilization oven (J.P Selecta, Spain) overnight at 50 °C and stored in a humidity controlled for further characterization. The drying stages of the recycled CAt are shown in Figure 3.

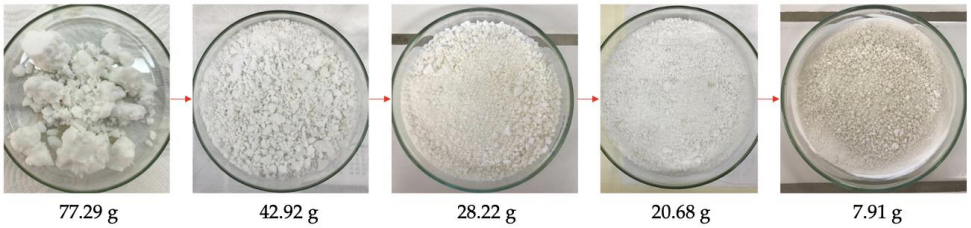

Figure 3. Demonstration of the drying process of recycled synthesized CAt.

The degree of acetylation was determined by acid-base titration. Firstly, 5.0 mL of NaOH (0.25 mol L1) and 5.0 mL of CH_3CH_2OH were added to 0.10 g of CAt and the mixture was left to stand for 24 hours. After 24 hours, 10 mL of HCl (0.25 mol L1) was added and the mixture was left to stand for 30 min. After this period, the solution was titrated with a standard NaOH solution, using $C_{20}H_{14}O_4$ as an indicator [37]. This test was carried out in triplicate. The percentage of acetyl groups (%GA) was obtained using the following Equation. (1):

$$\%GA = \frac{[(V_{bi} + V_{bt}).\mu b - (V_a.\mu a).M.100]}{mCAt} \quad (1)$$

where, V_{bi} is the volume of NaOH added to the system (L), V_{bt} is the volume of NaOH used in the titration (L), μb is the molarity of sodium hydroxide (M), V_a is the volume of HCl added to the system, μa is the molarity of hydrochloric acid (M), M is the molar mass of the acetyl group (g/mol) and $mCAt$ is the mass of the CAt sample (g). By performing the degree of acetylation, it is possible to determine the degree of substitution of the sample [38].

2.3. Fibres production

Solutions of CA (10-20-30 wt. %) and PEG2000 at (40-60-80 wt. %) were prepared overnight in DMF and dH_2O respectively, both stirred continuously at 50 °C. While the CAt (8 wt. %) solutions were prepared overnight in NMP under moderate stirring at 50 °C. Prior to the wet spinning production, the solutions were left to stand at room temperature for 1 h to remove any air bubbles.

For all productions, the wet spinning set-up consisted of a syringe pump NE- 1000 (New Era Pump Systems Inc, EUA) a coagulation bath composed of dH_2O at room temperature, a collector, a needle (uniaxial or coaxial and one/two syringes connected to the pump, being the latter two parameters adjusted according to the type of fibre produced. A representative schematic of the wet spinning process is shown in Figure 4. The Fibre collection consisted of an aluminium foil wrapped around the automatic collector at a moderate velocity of 6.21 rpm. The distance between the collector and the needle was 45 cm and the distance between the needle and the coagulation bath was 5 cm.

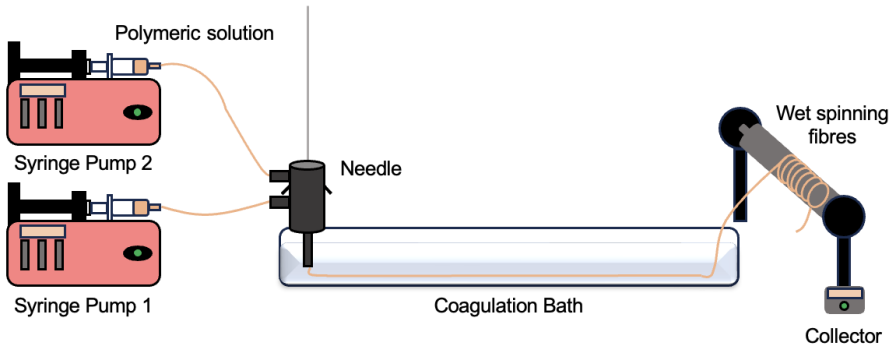

Figure 4. Scheme of production of PCFs via wet spinning.

 doi:10.20944/preprints202402.1278.v1

To produce uniaxial fibres (Fu) and uniaxial CAt fibres (Fut), the wet spinning configuration was applied, but the needle used for the process was uniaxial, requiring only one pump, adjusting according to ejection parameters. To produce hollow fibres (Fh), hollow CAt fibres (Fht), PCF and coaxial CAt fibres (PCFt), the only parameter that differed was the needle, which instead of being a single needle was replaced by a coaxial needle, while for Fh and Fht only the outermost port was used with the solution of CA and CAt, respectively. In contrast, for PCF and PCFt, the outermost port was used for CA and CAt, respectively, and the innermost port for PEG2000.

The parameters for the wet spinning process were adjusted to obtain fibres with better properties [39] and were demonstrated in Figure 5. The ejection velocity for CA was 0.165 mL/min, while for PEG2000, it varied from (0.130-0.140-0.150 mL/min). Fibres with CAt and PEG2000 were produced with slightly lower ejection velocities, namely 0.130 mL/min for CAt and (0.100-0.120 mL/min) for PEG2000. In the case of coaxial fibres, CAt used different ejection velocities to obtain enough time to compose the coaxial system with a protective sheath.

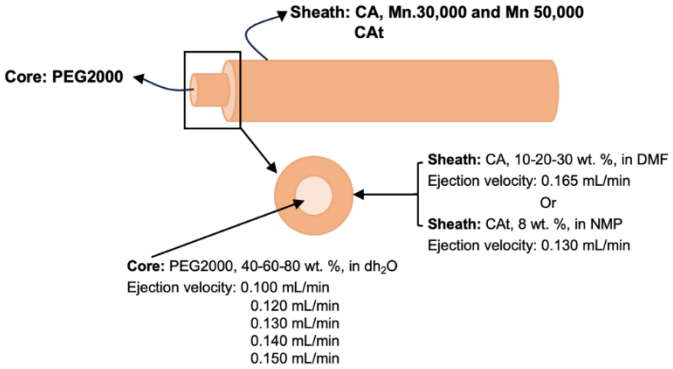

Figure 5. The parameters for the wet spinning process.

After production, all fibres were passed through dH_2O to remove any traces of solvent (DMF and NMP) and dried for 1 hour at room temperature. The fibres were then stored at room temperature and humidity for subsequent testing. A qualitative analysis was carried out during the production of the fibres by wet spinning, which considered whether the fibres could be extruded easily, whether there was surface roughness and whether the fibres were extruded uniformly. This analysis is presented in the results and discussions.

PEG, being soluble in dH_2O, guarantees its incorporation into the fibre. When the dH_2O meets the walls of the protective sheath, coagulation occurs, forming a resistant inner wall to fix the substance. Although there are not yet many reports on wet-spun coaxial fibres with this type of structure, it is hoped that research will progress in this direction.

2.4. Fibres physical, chemical, thermal and mechanical characterization

2.4.1. Bright-field microscopy

The morphology of the fibres will be presented. In addition, this test will give indications of the presence of a coaxial system. This analysis was carried out by bright-field microscopy using a Leica DM IL LED inverted microscope (Leica Microsystems, Weetzlar, Germany). Images were taken at 5x magnification, and the average fibres diameter was determined by ImageJ® software (version 1.53, National Institutes of Health, Bethesda, Maryland, USA).

2.4.2. Scanning Electron Microscopy (SEM)

To examine the morphology and differentiation between the fibre structure (uniaxial, hollow or coaxial), the CA and CAt sheath, along with the corresponding cores within the fibres, SEM micrographs fibres were characterised and obtained using a dual-column ultra-high resolution field emission SEM (NOVA 200 Nano SEM, FEI Company, Texas, USA) with an accelerating voltage of 10

 doi:10.20944/preprints202402.1278.v1

kV. The samples were initially coated with a 10 nm gold-palladium film (Au-Pd, 80-20% w/v) using a 208 High-Resolution Sputter-Coater (Cressington Company, Watford WD19 4BX, UK) coupled to an MTM-20 High-Resolution Thickness Controller (Cressington Company). Images were taken at 500× magnification.

2.4.3. Attenuated Total Reflectance-Fourier Transform Infrared spectroscopy (ATR-FTIR)

Surface chemistry and chemical composition of different fibres were analysed using attenuated total reflectance Fourier transform infrared spectroscopy (ATR-FTIR). The equipment used was an IRAffinity-1S (Shimadzu, Kyoto, Japan), coupled with a HATR 10 accessory with a diamond crystal. The spectra were obtained over a wavenumber range of 400-4000 cm^{-1} at a scanning velocity of 200 scans with a resolution of 2 cm^{-1}.

2.4.4. Thermogravimetric Analysis (TGA)

Thermogravimetric analyses (TGA) to evaluate variations in the thermal stability of polymers materials, specifically CA (Mn 30,000 and 50,000), recycled CAt and PEG2000, and samples of fibres were carried out using Hitachi STA 7200 equipment (Fukuoka, Japan). The samples were placed in platinum crucible (Mettler Toledo, ME-26763, Columbus, USA) and exposed to a heating rate of 10 °C/min over a range of 25 to 500 °C for all samples. The measurements were carried out under a N_2 atmosphere of 200 mL/min. The test was carried out using an empty crucible as a reference.

2.4.5. Differential Scanning Calorimetry (DSC)

To evaluate the phase change behaviour of the samples, verifying the phase change temperature, the melting enthalpy and the endothermic changes of the materials, specifically CA (Mn 30,000 and 50,000), recycled CAt and PEG2000, and the fibre samples, DSC analyses were carried out using Mettler Toledo equipment, model DSC-822 (Columbus, USA), and a cooling accessory (Labplant RP-60 cryostat, Huddersfield, UK). The polymers materials samples were placed in an aluminium crucible (Mettler Toledo, ME-26763, Columbus, USA) and exposed to a heating rate of 10 °C/min over a range of 25 to 500 °C for all samples under an N_2 atmosphere of 200 mL/min.

2.4.6. Mechanical Performance – Dynamometer

The mechanical properties of the fibres were evaluated under tensile strength using the dynamometer test. The tensile strength and the maximum elongations of the fibres were determined using a Housefield H5KS dynamometer (Artilab, Kerkdriel, Netherlands), associated with the QMAT Materials Testing & Analysis software, following the ISO 2062 - 2009 standard. Fibres with 10 cm long were analysed at RT with a holding distance, also known as gauge length, starting at 100 mm and increasing continuously until the maximum elongation to break was reached. The extension range was 5 mm, and the crosshead velocity was set at 25 mm/min, using a load cell of 250 N, applied with a preload of 0 N and a load interval of 100 N.

3. Results

3.1. Degree of substitution for CAt

The process of verifying the degree of substitution for the CAt was carried out by initially separating 0.1 g of the recycled CAt in a flask and adding 5 mL of NaOH solution (0.25 mol/L) and 5 mL of absolute ethanol. After the samples had rested for 24 hours, 10 mL of HCl solution (0.25 mol/L) was added and left to rest for 30 minutes. Finally, 3 drops of phenolphthalein solution were added to each of the samples and the acid-base titration was carried out by shaking the samples and using the standardised NaOH (0.25 mol/L) solution until a pink colour was reached. Puleo *et al.* (1989) stated that by calculating the degree of acetylation (%GA), it is possible to determine the degree of substitution of the CAt, since for a degree of substitution (DS) of 2.88 a %GA of 43.5% is associated [38]. Thus, the DS of the CAt samples was calculated, and the results are shown in Table 1.

 doi:10.20944/preprints202402.1278.v1

Table 1. Degree of acetylation and degree of substitution for CAt synthesized.

Samples	%GA	DS
CAt	42.70	2.83
CAt_1	42.74	2.83
CAt_2	42.96	2.84
Average	42.80 ± 0.14[1]	2.83 ± 0.01[1]

[1] Standard deviation.

As can be seen, the recycled CAt showed a DS very similar to the theory, of ≈ 2.83, and a %GA of 42.80%. These results show that the acetyl groups partially replaced the hydroxyl groups through an acetylation reaction, making it possible to obtain the recycled CAt. These results are in line with those of the commercial samples. CA is the most important ester of cellulose, with the OH groups of cellulose being replaced with acetyl groups at a DS of approximately 2.50 [40].

During the testing of the DS of recycled CAt, it was shown that there can be a large amount of intermolecular interaction between the two hydroxyl groups, between two acetyl groups and between the hydroxyl and an acetyl. These intermolecular interactions contribute to the packing and movement of the cellulose acetate chains. Since all positions are approximately uniformly acetylated, the type and number of intermolecular interactions are also distributed uniformly throughout the polymer [38]. Therefore, since the results obtained, recycled CAt can be tested in the manufacture of fibres.

3.2. Fibres production

The different (functionalized) fibre samples were designated by an alphanumeric string Table 2, called Fu_a_b, Fh_a_b and PCF_a_b/x_y for the fibres with CA/PEG2000 and Fut_b, Fht_b and PCFt_b/x_y for the fibres with CAt/PEG2000. Starting with Fu, Fut, Fh, Fht, PCF and PCFt to indicate the type of fibre, respectively uniaxial, recycled uniaxial, hollow, recycled hollow, phase change fibres and recycled phase change fibres. Next, the letter a represents the molecular weight (Mn 30,000 or Mn 50,000) of the CA, the letter b represents the concentration of CA (10-20-30 wt. %) and CAt (8 wt. %), the letter x represents the concentration of PEG2000 (40-60-80 wt. %) and, finally, the letter y represents the ejection velocity of PEG2000 (0.100-0.120-0.130-0.140-0.150 mL/min). In this case, the concentration of the solvent DMF, the solvent NMP, the ejection velocity of CA (0.165 mL/min), the ejection velocity of CAt (0.130 mL/min) and the molecular weight of PEG (Mn 2000) were not represented in the alphanumeric string of the samples, as they are constant values. For example, PCF_30_30/40_140, where it represents the structure PCF_a_b/x_y, i.e. PCF is the designation for a phase change fibre, the letter a is 30, the molecular weight of the CA (Mn 30,000), the letter b is 30, 30% concentration of the CA solution, the letter x is 40, 40% concentration of the PEG2000 solution and, finally, the letter y is 140, 0.140 mL/min ejection velocity of the PEG2000.

Table 2. Name of the samples for the wet spinning process.

Samples	Fibre Type	Mn CA	wt. % CA/CAt	wt. % PEG	Ejection Velocity PEG (mL/min)
Fu_a_b	Uniaxial	30,000 and 50,000	10, 20 and 30	-	-
Fut_b	Uniaxial	-	8	-	-
Fh_a_b	Hollow	30,000 and 50,000	10, 20 and 30	-	-
Fht_b	Hollow	-	8	-	-
PCF_a_b/x_y	Phase Change Fibre	30,000 and 50,000	10, 20 and 30	40,60 and 80	0.130, 0.140 and 0.150

 doi:10.20944/preprints202402.1278.v1

PCFt_b/x_y	Phase Change Fibre	-	8	40 and 80	0.100 and 0.120

While producing the fibres by wet spinning, it was important to pay attention and record whether the fibres were produced uniformly or presented any defects, which would condition future testing. Table S3 reports the observations.

In this study, the production of recycled fibres made from CAt in the sheath and PEG2000 in the core was considered by testing only to produce the fibres under the same conditions as the commercial one with the best results.

3.3. Sample selection

Before starting to analyse the results, a flowchart was drawn up (Figure 6) showing production with CA in the sheath and PEG2000 in the core. This flowchart considered the number of samples produced and their variables. This approach aimed to better organise and justify the choice of the best conditions for carrying out both the production of the samples with recycled CA and the more detailed tests, such as dynamometry, DSC and TGA, planned for this article.

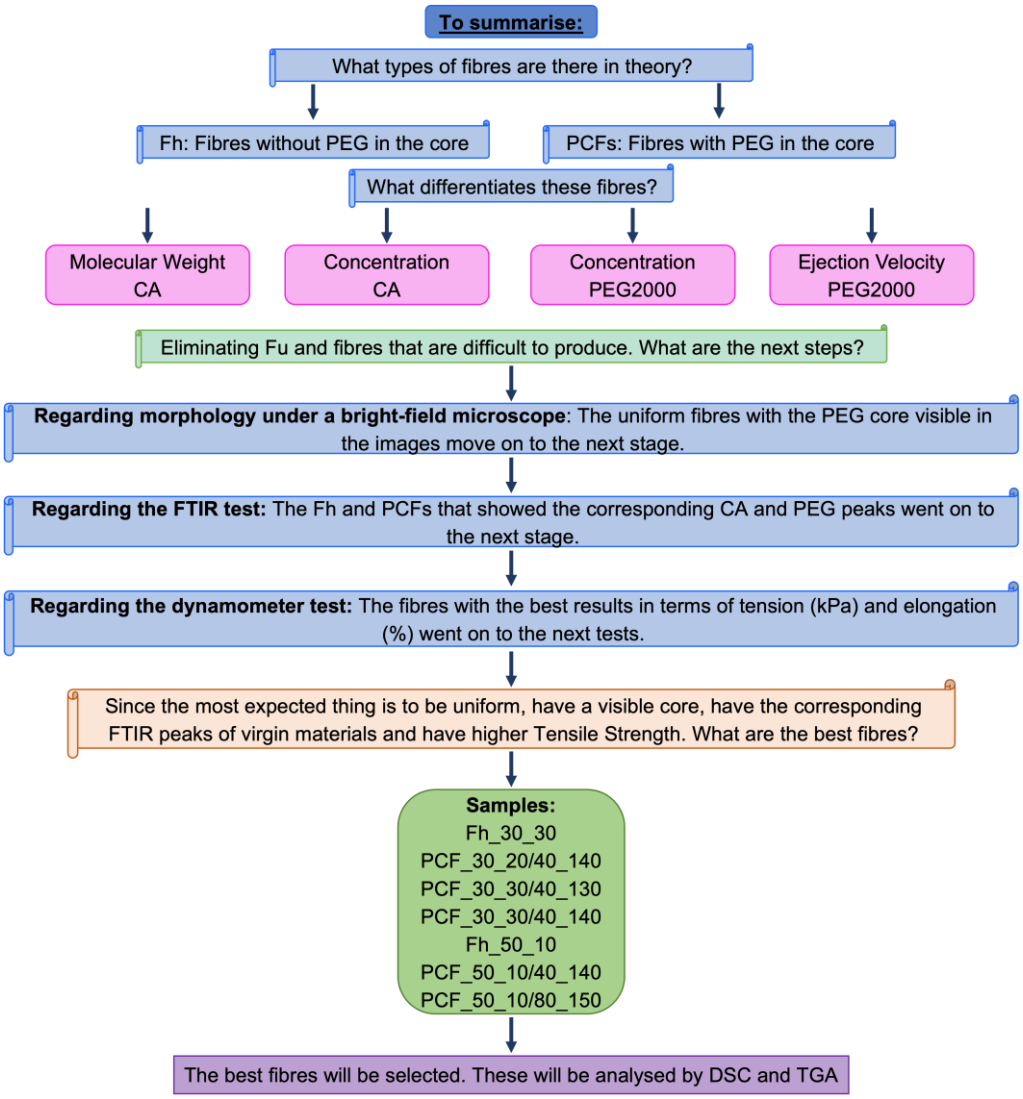

Figure 6. A flowchart explaining the selection of the best samples.

The flowchart indicated that the samples with 40% and 80% PEG2000 performed better than the remainder. Therefore, the production of the fibres with recycled CAt followed the same conditions.

 doi:10.20944/preprints202402.1278.v1

In addition to Fut and Fht, PCFt was produced with 40% and 80% PEG2000. The ejection velocities were set at 0.100 mL/ min for 40% and 0.120 mL/min for 80% for both CA and CAt.

3.4. Morphology

At this point, only the fibres with the best performance in terms of wet spinning production were analysed. Figure 7 illustrates the morphology of these 13 fibres, where direct observation revealed that PCFs_30_30 have a more rounded, cylindrical shape. This can be explained by the differences in concentration, 30 wt.% (Mn 30,000) versus 10 wt.% (Mn 50,000). The production of PCFt with recycled CA in the sheath and PEG2000 in the core was an innovation that encompassed everything from the solution phase to ejection by wet spinning.

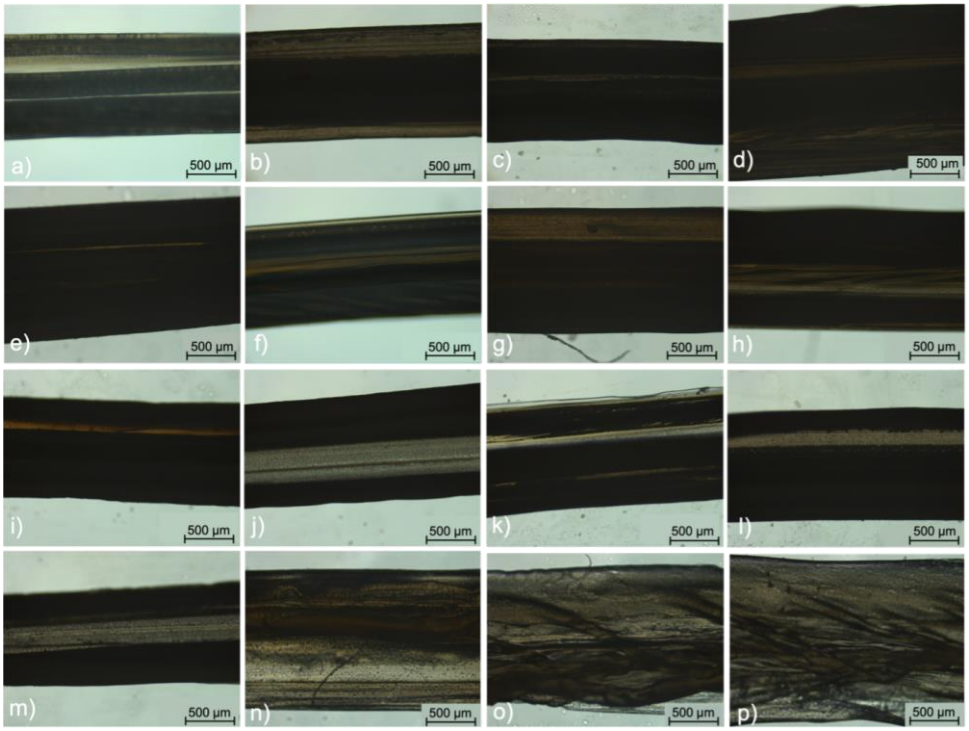

Figure 7. Micrographs of the morphology of the hollow and PEG2000 incorporated fibres obtained by brightfield microscopy. (**a**) Fh_30_30; (**b**) PCF_30_10/60_150; (**c**) PCF_30_10/80_150; (**d**) PCF_30_20/40_140; **(e**) PCF_30_30/40_130; (**f**) PCF_30_30/40_140; (**g**) PCF_30_30/40_150; (**h**) PCF_30_30/80_150; (**i**) Fh_50_10; (**j**) PCF_50_10/40_130; **(k**) PCF_50_10/40_140; (**l**) PCF_50_10/80_140; (**m**) PCF_50_10/80_150; (**n**) Fht_8; (**o**) PCFt_8/40_100; (**p**) PCFt_8/80_120.

These fibres were then measured for thickness (Figure 8) using ImageJ software. As can be seen in Figure 8, of the 29 fibres analysed, only 13 had a uniform morphology and a visible core. The main difference between CA with Mn 30,000 and Mn 50,000 is in the molar mass of the CA molecules [41,42]. In more practical terms, this difference in molar mass can affect the material's properties, such as its solubility, viscosity and mechanical strength.

Preprints.org (www.preprints.org) | NOT PEER-REVIEWED | Posted: 22 February 2024 doi:10.20944/preprints202402.1278.v1

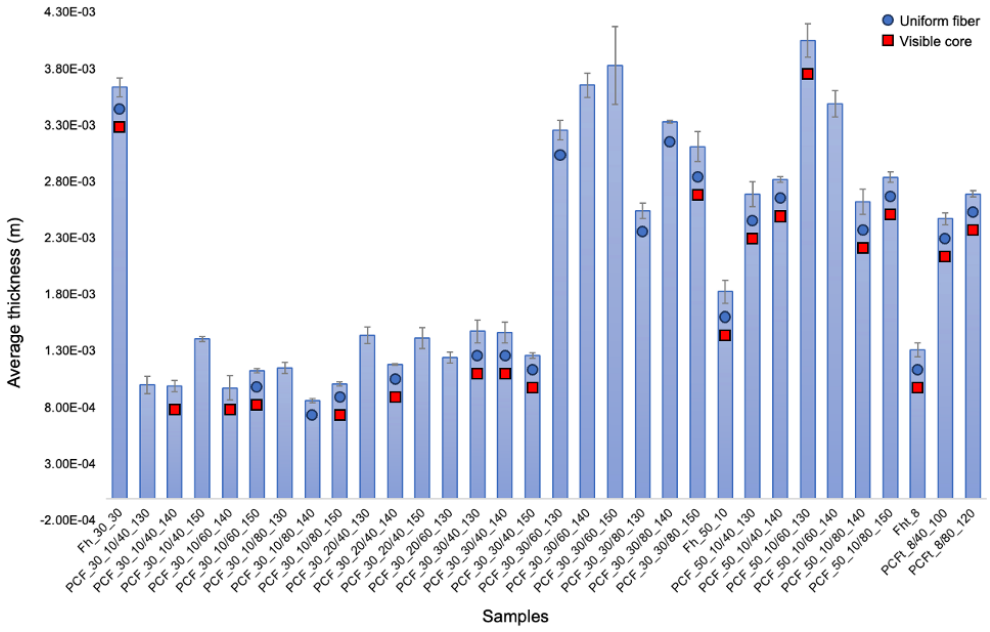

Figure 8. Calculation of the thickness of the fibres produced by wet spinning with a detailed analysis of the uniformity and presence of the visible core. Data presented as mean ± SD (n = 5).

The different types of fibre structure were observed by SEM in Figure 9. In general, the structures have an expected shape, where Fu, uniaxial, has a cylindrical structure. In comparison, Fh has a coaxial hole, albeit a small one, which could be affected by the fact that it was filled with dH_2O and when it met the coagulation bath, as it did not have a core structure, the structure collapsed and flattened. The PCF composed of CA (Mn 30,000) in the sheath and PEG2000 in the core had a more cylindrical structure with a larger opening, compared to the PCF composed of CA (Mn 50,000) in the sheath and PEG2000 in the core, which not only had a smaller coaxial but also a flattened structure. In addition, the PCFt with a PEG2000 with 80% concentration in the core showed a similar, albeit less uniform, structure to the PCF_50 with the same PEG2000 concentration.

The presence of PEG2000 inside the PCFs is not noticeable and can be explained by a few possible factors. Firstly, as PEG2000 is diluted in dH_2O and is in liquid form, when cutting the PCFs samples for SEM, the PEG could leak out. Another viable option is the potential evaporation of the polymer during vacuum. It is also likely, that the magnification of the test was not big enough to detect the PEG2000 in contact with the CA and CAt sheath. Even though PEG detection was not possible, the goal of this test was the visualisation of the coaxial fibres, which was achieved.

 doi:10.20944/preprints202402.1278.v1

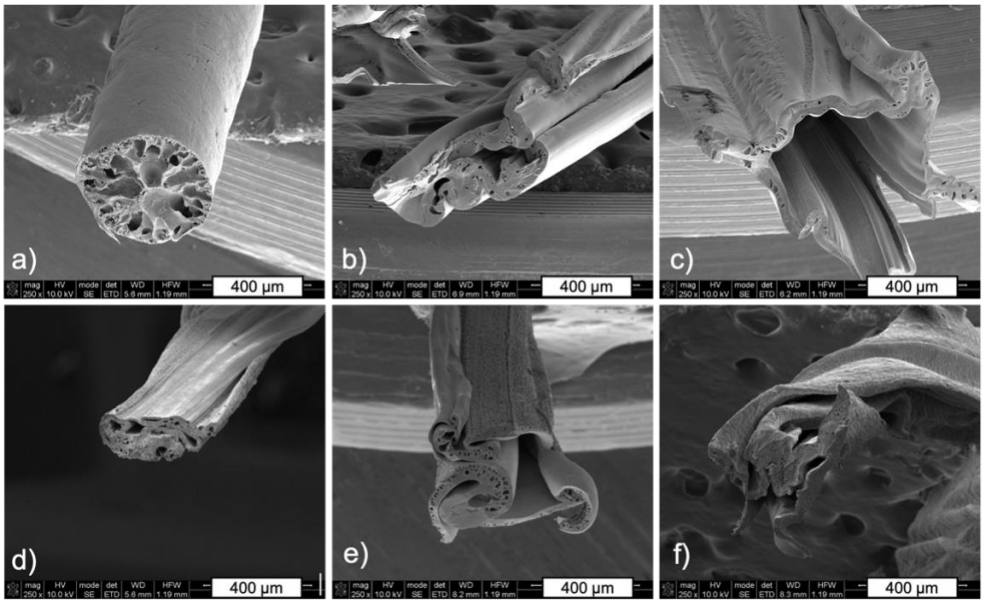

Figure 9. SEM micrographs of the Fu, Fh, PCF and PCFt. (**a**) Fu_30_30; (**b**) Fh_30_30; (**c**) PCF_30_30/40_140; (**d**) PCF_50_10/40_140; (**e**) PCF_50_10/80_150; (**f**) PCFt_8/40_100.

3.5. Chemical Composition (ATR-FTIR)

ATR-FTIR was used to investigate the chemical composition of the hollow and uniaxial fibres derived from CA [43,44]. The obtained spectra revealed characteristic peaks, mainly at 1745, 1657, 1376, 1238, 1047, and 901 cm^{-1}, indicating the prevalent bonds and functional groups within these fibres [45]. The 1745 cm^{-1} peak was attributed to the stretching vibration of the carbonyl group (C=O) from acetate units, signalling the successful acetylation [46]. A peak near 1657 cm^{-1}, approximating the expected band for C=O stretching in DMF around 1670 cm^{-1}, refers to a potential residual solvent within the resultant fibres [43]. Furthermore, peaks at 1376 and 1238 cm^{-1} were ascribed to the symmetric deformation vibrations of CH3 in the acetate units and the ester linkage C-O-C stretching in the CA molecule, respectively [47]. A band at 1047 cm^{-1} confirmed the presence of typical C-O stretching vibrations found in cellulose derivatives, further affirming the structural integrity post-fibre fabrication [43]. The 901 cm^{-1} peak is characteristic of the glycosidic ring's out-of-plane vibration, cementing the fibre's polysaccharide character [48].

ATR-FTIR also provided detailed chemical structure analyses of the coaxial fibres comprising a CA sheath enveloping a PEG2000 core (Figure 10a,b). The analysis exhibited noticeable peaks, offering insights into molecular interactions and functional groups within the fibre. The 2885 cm^{-1} peak resonated with C-H stretching vibrations of methyl (-CH3) and methylene (-CH2-) groups, aligning with PEG2000 repetitive methylene units and cellulose acetate's structural attributes [49]. A 1745 cm^{-1} peak corresponded to the C=O stretching vibration characteristic of the acetate groups bonded with the cellulose polymer, underlining the seamless incorporation of the acetate structure [46]. The peak at 1657 cm^{-1} is notable; while it aligns with C=O stretching vibrations, potentially emanating from residual DMF, it also alludes to potential contributions from PEG, precisely any traces of water or -OH group deformations [50]. Peaks observed at 1465, 1376, and 1368 cm^{-1} match with the structural vibrations of PEG2000 and acetate groups, signifying methylene deformation and methyl symmetric deformations, respectively [51]. Additionally, peaks at 1278, 1238, and 1105 cm^{-1} can be tied to varied C-O and C-O-C stretching, denoting the ester connections in cellulose acetate and PEG2000 recurrent ether linkages [52]. Peaks at 1047, 939, and 901 cm^{-1} further cement the polysaccharide nature of the fibre, with the latter denoting the glycosidic ring's out-of-plane vibration in cellulose structures [52]. The 835 cm^{-1} peak might have origins in the PEG framework [49].

The FTIR analysis of the recycled CAt and its respective spectra are shown in Figure 10c. As can be seen, the spectrum for the CAt recycled is very similar to the spectrum of the commercial CA.

 doi:10.20944/preprints202402.1278.v1

There is a pronounced band at 1748 cm^{-1}, which may be due to the stretching of the ester's carbonyl, a characteristic of acetyl groups. Based on the literature, this peak is one of the main indications that cellulose has been acetylated [53]. It is also possible to see the presence of a band between 1300 and 1200 cm^{-1} (peak at 1238 cm^{-1}), which represents the C-O stretching of acetate. The appearance of the band at 1376 cm^{-1} corresponds to the vibration of the C-H bond, which is also a characteristic band of acetyl groups. Therefore, the ATR-FTIR spectra indicate that acetylation of the cellulose molecule has been successfully carried out [54].

 doi:10.20944/preprints202402.1278.v1

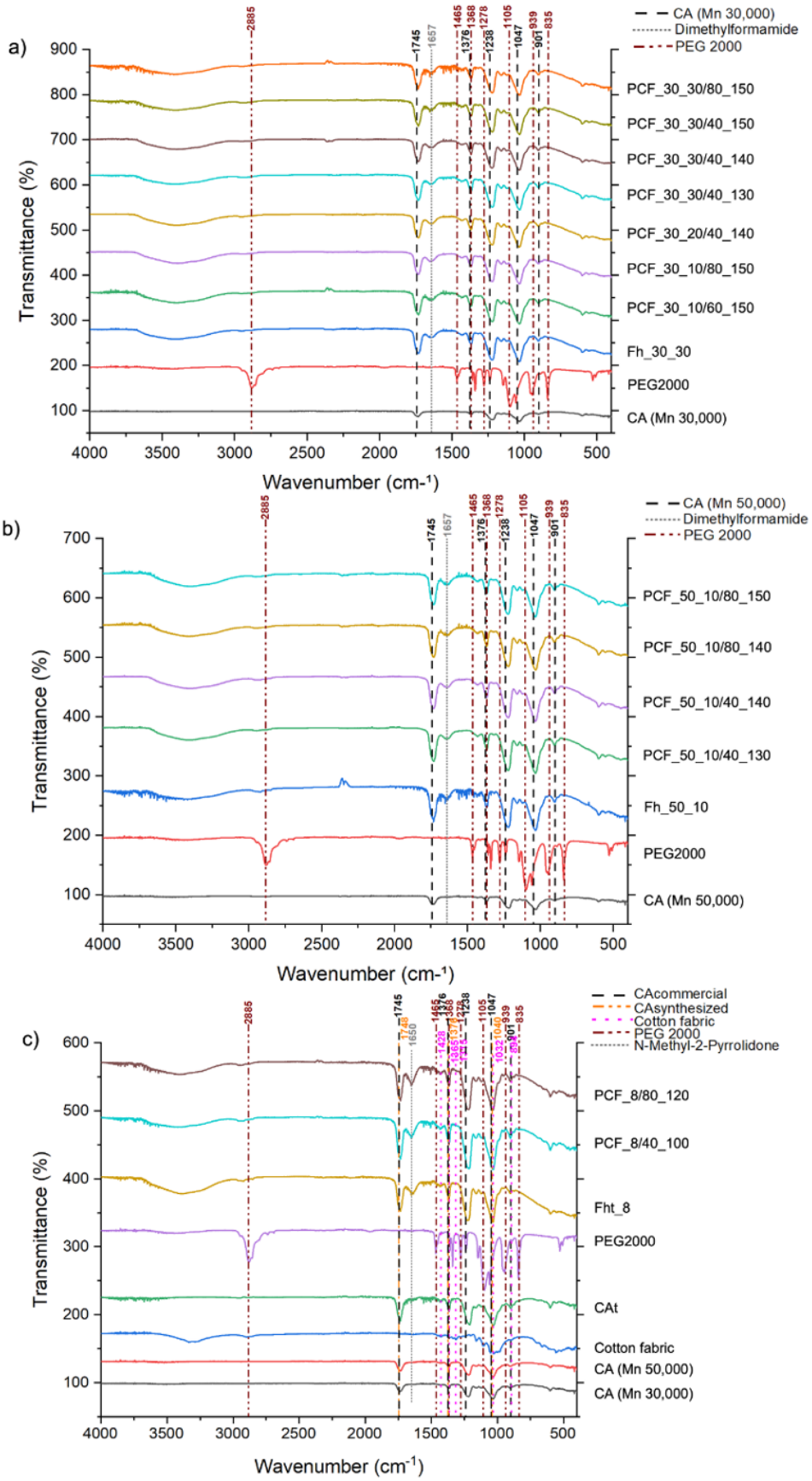

Figure 10. ATR-FTIR spectra of (**a**) Fh_30, PCF_30_10, PCF_30_20 and PCF_30_30 fibres; (**b**) Fh_50_10 and PCF_50_10 fibres; (**c**) CAt, Fht and PCFt fibres.

 doi:10.20944/preprints202402.1278.v1

3.6. Thermogravimetric Analysis (TGA)

The increase in temperature associated with polymer degradation was identified in the variations in the fibres' TGA curves, as shown in Figure 11. In the initial phase, degradation was observed up to ≈ 100 °C in all the samples, this phase corresponding to the dehydration of the samples with the elimination of the dH_2O molecules (associated with humidity) [55] and potential traces of DMF and NMP solvents. As mentioned in the materials and methods section, the fibres were stored for 24 h in a humidity-controlled environment and, to maintain their integrity, they were subjected to TGA without the fibres being completely free of dH_2O. Both the Fh and the PCFs showed thermal stability up to ≈ 300 °C and ≈ 350 °C, respectively. Thereafter, mass losses were observed, consistent with the endothermic peak recorded in the DSC around 415 °C (Figure 12) [56]. The fact that PCFs, which have a CA sheath and a PEG core, showed thermal stability followed by mass loss at a slightly higher temperature can be explained by the presence of PEG in their core. Thus, the decomposition of the polymer takes place in two phases, with the first degradation due to the breakdown of the PEG2000 chains and the second decomposition due to the breakdown of CA [57]. According to the literature, the pyrolysis process of PEG with a molecular weight above 1000 g/mol generally takes place at a temperature of 350 °C, where thermal decomposition begins at the -C-O- and -C-C- bonds of the two chains and is evident between 340 and 415 °C [58]. However, CA has high thermal stability, with a degradation temperature of over 300 °C [57].

Considering that the PCFs with the best performance were selected, both visually and through mechanical and thermal tests, the results presented by the TGA analysis may be associated with the diameter of the PCFs. The PCFs with Mn 30,000 CA in the sheath had a more cylindrical shape, thus better preserving the PEG at their core, while the PCFs with Mn 50,000 CA showed flattening, which may have compromised the thermal stability of the PCFs (as evidenced in the DSC data) and resulted in a slightly greater loss of mass [24].

Finally, about the TGA analysis for PCFt, as with the PCFs, degradation up to ≈ 100 °C was recognized in all the samples, where the extent of this step corresponds to the dehydration of the samples with the elimination of the dH_2O molecules and the NMP solvent present during production. CA synthesized with a degree of substitution of 2.90 registers the most important degradation step at 350-360 °C [54,59]. Therefore, the results for PCFt with a degree of substitution of 2.83 are in line with the literature and show similar thermal behaviour with a degradation temperature of ≈ 350 °C.

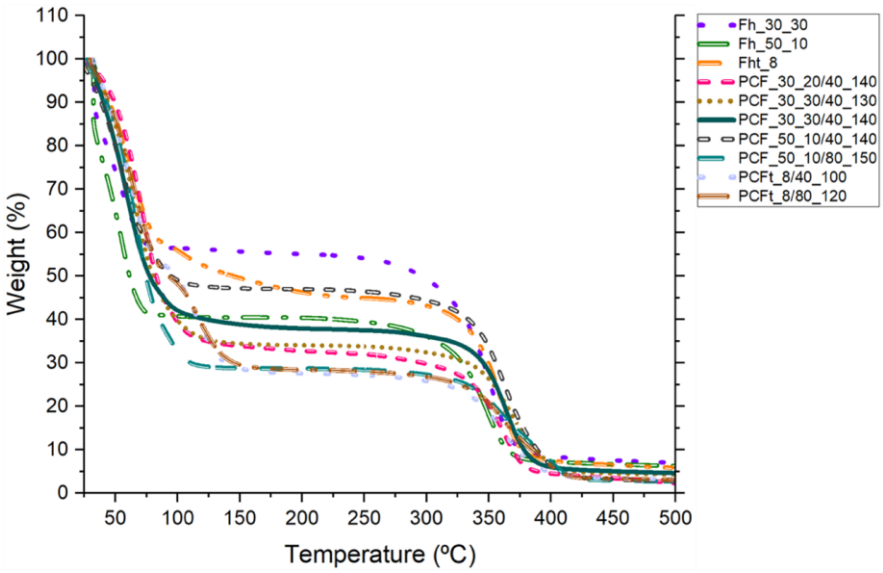

Figure 1. TGA curves of the Fh, PCF, Fht and PCFt fibres, obtained from 25 to 500 ◦C under nitrogen atmosphere, flow rate of 200 mL/min and temperature rise of 10 °C/min.

3.7. Differential Scanning Calorimetry (DSC)

 doi:10.20944/preprints202402.1278.v1

Bulleted lists look like this: DSC is used to study the thermal behaviour of materials and to determine enthalpy [33]. Figure 12 hows the DSC thermograms for Fh, Fht, PCFs and PCFts, in which coaxial fibres have different CA molecular weights and concentrations and different PEG concentrations and ejection velocities. Meanwhile, the corresponding thermal property data from the DSC curves are shown in **Error! Reference source not found.**.

At first, both Fh and Fht were subjected to DSC and, as can be seen in Figure 13, an average endothermic transition occurred around 100 °C, which suggests the loss of moisture absorbed from the solvents [20] and the elimination of water molecules [60]. An average peak at ≈ 137.26 ºC was detected and associated with the glass transition temperature of CA [61]. Finally, a last peak was detected at ≈ 236.08 ºC, which was attributed to the crystallisation of the amorphous domains of the CA chains [60].

When the PCFs and PCFts were subjected to the DSC test, a different behaviour was seen, where the addition of PEG to the core of the CA and CAt fibres resulted in the appearance of an average endothermic transition at ≈ 38.30 ºC and an average peak, representative of PEG, at around 70.72 °C, with a variation of 10 ºC, which is attributed to the exothermic crystallisation of PEG [62].

A peak at ≈ 89.25 ºC was also observed because of the interactions between CA, CAt and PEG, which displaced the peak detected in the pristine CA fibres at 92 ºC. The introduction of a plasticiser such as PEG into the core lowers the Tg of the CA polymer as it causes a reduction in intermolecular forces, generating protective effects with functional groups such as -OH [34]. The PEG acts as a working material and the CA entanglement, due to secondary interactions, hinders and disturbs the orientation of the PEG molecular chains [57]. This explains the displacement of the endothermic melting peak of PEG2000 crystallisation, since according to A.K. Ansu *et al.*, this peak normally occurs in the 46-54 ºC range. These interactions between the carbonyl of CA and the hydroxyl groups of PEG occur frequently and this justifies the displacement of the characteristic PEG peak [62,63]. Finally, two endothermic peaks could still be observed, the first characteristic of CA and CAt at ≈ 223.85 ºC and the second referring to the PEG pyrolysis process at ≈ 370.55 ºC, which generally happens around 350 ºC, as detailed in the TGA discussion. As reported, the higher the molecular weight of PEG, the higher the temperature at which the pyrolysis process takes place, which explains the increase of ≈ 20.55 ºC [58].

The peaks around 70 °C determined the enthalpy of phase change (Table 4). This reduction in PEG's enthalpy of phase change was due to the disturbance in PEG crystallisation caused by the presence of CA [57]. There is a protective CA sheath, which, due to the different molecular weights and concentrations, was better formed for PCFs_30_30 and, consequently, PEG used less energy to change phases. Meanwhile, for PCF_50_10, as the sheath was less developed and the PCF was flatter, PEG needed more energy to change the phase. This explains why the enthalpy values were lower for PCFs_30_30. Therefore, the corresponding experimental enthalpy values for PCFs_30_30 were lower than the theoretical ones, with the decrease in enthalpy being attributed to PEG crystallisation becoming restricted and the possible entanglement between the PEG and CA molecular chains in the sheath of PCFs and PCFt [64]. Another factor that may have influenced this was the use of different PEG concentrations, i.e. even with a lower concentration for most of the PCFs, the high temperature was able to distribute the solution evenly, so that crystallisation was not negatively affected [57]. Finally, PCFs have good thermal reliability due to the PEG in the core of the fibres, as discussed above.

 doi:10.20944/preprints202402.1278.v1

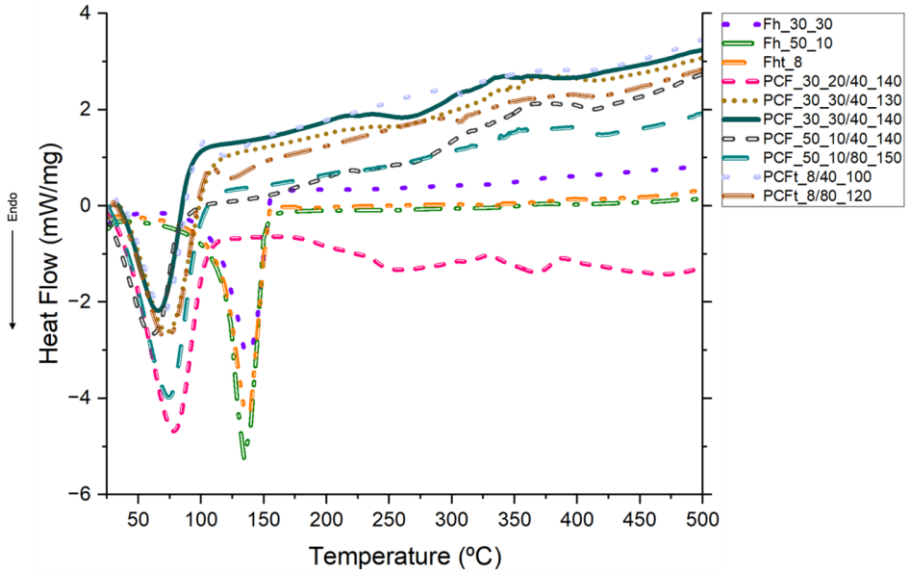

Figure 12. DSC curves of the Fh, PCF, Fht and PCFt fibres, obtained from 25 to 500 ◦C under nitrogen atmosphere, flow rate of 200 mL/min and temperature rise of 10 °C/min.

Table 4. Thermal properties of Fh, Fht, PCF and PCFt.

Samples	Peak Temperature (°C)	Melting Point (J/g)
Fh_30_30	139.84	111.78
Fh_50_10	134.42	140.46
Fht_8	137.52	134.39
PCF_30_20/40_140	78.02	108.43
PCF_30_30/40_130	72.26	56.38
PCF_30_30/40_140	64.87	50.51
PCF_50_10/40_140	61.61	70.91
PCF_50_10/80_150	74.96	106.40
PCFt_8/40_100	69.83	44.97
PCFt_8/80_120	72.84	41.52

3.8. Mechanical behavior

The maximum elongation and maximum breaking strength of the Fh and PCF fibres produced by wet spinning were analysed using 10 cm long filaments (Table 5). This test was carried out to assess and observe the mechanical strength of the fibres.

The fibres that did not show uniformity and a visible core could not be examined, since after the production, they were flattened and open, because of the fibre collapsing into its hollow interiorand possible clogging of the needle, respectively.

Table 5. Mechanical testing of wet spinning fibres. Data presented as mean ± SD (n = 5).

Samples	Maximum elongations at break (%)	Breaking strength (kPa)
Fh_30_30	28.86 ± 1.59	133.18 ± 6.57
PCF_30_10/60_150	1.59 ± 0.14	105.54 ± 14.73
PCF_30_10/80_150	2.46 ± 0.30	212.83 ± 52.80
PCF_30_20/40_140	14.32 ± 0.22	1023.64 ± 52.56
PCF_30_30/40_130	28.46 ± 1.08	1094.60 ± 150.04
PCF_30_30/40_140	22.42 ± 0.84	1122.49 ± 145.56
PCF_30_30/40_150	13.07 ± 0.93	920.01 ± 104.02
PCF_30_30/80_150	25.40 ± 0.63	264.68 ± 22.18

 doi:10.20944/preprints202402.1278.v1

Samples	Maximum elongations at break (%)	Breaking strength (kPa)
Fh_50_10	16.50 ± 0.95	117.28 ± 30.03
PCF_50_10/40_130	11.71 ± 0.60	60.28 ± 5.86
PCF_50_10/40_140	16.20 ± 0.99	100.63 ± 13.22
PCF_50_10/80_140	12.98 ± 0.58	75.03 ± 17.68
PCF_50_10/80_150	21.62 ± 0.42	105.69 ± 15.68
Fht_8	4.00 ± 0.71	61.36 ± 18.46
PCFt_8/40_100	7.18 ± 0.62	28.06 ± 14.20
PCFt_8/80_120	9.02 ± 0.66	39.75 ± 9.21

Reports have addressed the poor mechanical properties of CA alone as an obstacle for many applications [65]. However, this does not significantly influence PCFs, since the final application depends on the properties of the CA, PEG and PCF composites working together.

The tensile properties of wet-spun fibres can be affected by different factors, from the concentration of the CA, the direction of the test, the concentration of the solution and so on [34].

In this work, the tensile properties of PCFs and PCFt composed of CA and Cat in the sheath, respectively, and PEG2000 in the core were measured, examining the extent to which the concentrations of CA and PEG can influence the final data. The cross-sectional area of the fibres was measured using a bright-field microscopy (Figure 8) and from those values, the stress (kPa) could be calculated for each of the fibres. The maximum stress-stretch values for Fh and PCFs are shown in Table 5.

The mechanical properties of PCFs are also sensitive to the acetyl content; tensile strength and modulus of elasticity are higher in CA with lower molecular weights and higher concentrations. This indicates that increased acetylation produces a stronger and stiffer material. The glass transition decreases as the degree of acetylation increases, reflecting the reduced fraction of the amorphous phase [38]. Following the reasoning in the literature, comparisons between PCFs, where the difference was in the molecular weight of the CA, showed that fibres with a molecular weight of Mn 30,000 exhibit higher tensions, while fibres with Mn 50,000 show considerably lower values. This discrepancy can be attributed to the fact that PCF_30_30 has a thicker and better formed sheath compared to PCF_50_10. As for the comparison between the PCFs, where what changes is the concentration of CA, the conclusion is that the higher the concentration of CA, the values of elongation and tension increase. When the comparison factor is the concentration of PEG2000, what can be observed is that the lowest concentration, 40%, showed better results than the higher concentrations. Finally, the PEG ejection velocity was peculiar, while the moderate PEG velocity (0.140 mL/min) showed considerably higher values. This can be explained by the fact that, during fibre production, a moderate ejection speed (0.140 mL/min) can mean that the PEG does not mix with the CA sheath, remaining stored inside and considerably increasing the tension values [33]. As shown and discussed above, the PCFt had a less uniform morphology and structure and because of that, these fibres were more fragile and reported much lower values than expected compared to PCFs with commercial CA.

Therefore, the fibre with the highest tension value was PCF_30_30/40_140, which met all the requirements of the previous analyses.

5. Conclusions

In this study, an innovative approach was used to produce coaxial fibres using the wet spinning technique. These fibres were composed of cellulose acetate (CA) in the sheath, with different molecular weights and concentrations, while the core was made up of polyethylene glycol 2000 (PEG2000) with different concentrations and ejection speeds. The research aimed to improve the thermal properties of these fibres for potential applications in Civil Engineering. Chemical, thermal and mechanical tests were conducted to investigate the presence and impact of PEG2000 on the fibres. The results confirmed the successful production of coaxial fibres (PCFs) and the synthesis of recycled

 doi:10.20944/preprints202402.1278.v1

cellulose acetate (CAt). Microscopic analyses, including bright-field microscopy and scanning electron microscopy (SEM), differentiated between the core and the sheath, confirming the existence of coaxial fibres. Despite the challenges in confirming the presence of PEG2000 by SEM due to its liquid state, ATR-FTIR analyses showed representative peaks for CA, CAt and PEG2000 in all PCFs. Thermal tests (TGA and DSC) confirmed the presence of PEG2000, with the CA sheath influencing the displacement of the phase change peak and the decrease in PEG2000 enthalpy. The mechanical tests revealed varied performance between the fibres, with PCF_30_30 exhibiting superior tensile properties. The presence of PEG2000 was shown to improve the fibres' performance in terms of tension. The next step suggests optimising the wet spinning production system for a more uniform fibre morphology and structure, exploring alternative solvents, coagulation baths and addressing drying processes to avoid mass loss at high temperatures. These improvements aim to enhance fibre consistency, which is fundamental for civil engineering applications that require a phase change between 50-60 °C.

Supplementary Materials: The following supporting information can be downloaded at the website of this paper posted on Preprints.org, Table S3: Qualitative analysis of the production of the fibres.

Author Contributions: Conceptualisation, N.H., and N.C.H.; methodology, I.R.S., and N.C.H.; software, N.H., C.P., and M.M.P.S.; validation, J.A.O.C.; formal analysis, N.H., I.R.S., N.C.H., and H.P.F.; research, N.H., I.R.S., and J.A.O.C.; resources, H.P.F., M.F.M.C., and J.A.O.C.; data curation, N.H., C.P., and M.F.M.C.; preparation of the original draft, N.H.; revision and editing of the writing, C.P., I.R.S., N.C.H., M.M.P.S., H.P.F., G.M.B.S., E.F., M.F.M.C., and J.A.O.C.; visualisation, I.R.S., and N.C.H.; supervision, I.R.S., M.F.M.C., and J.A.O.C.; project administration, M.F.M.C., and J.A.O.C.; acquisition of funding, M.F.M.C., and J.A.O.C.; All authors have read and agreed with the published version of the manuscript.

Funding: This research was funded by the Portuguese Foundation for Science and Technology (FCT) under the projects MicroCoolPav EXPL/EQUEQU/1110/2021, NanoAir PTDC/FISMAC/6606/2020 and within the framework of Strategic Funding UIDB/04650/2020, UIDB/04029/2020 and UID/QUI/0686/2020. I.R.S and H.P.F would like to thank FCT for funding contracts 2022.00763.CEECIND and 2021.02720.CEECIND.

Acknowledgements: The authors would like to thank the company Nostrobiz for supplying 100% cotton fabrics.

References

1. Segundo, I.R.; Freitas, E.; Branco, V.T.F.C.; Landi, S.; Costa, M.F.; Carneiro, J.O. Review and Analysis of Advances in Functionalized, Smart, and Multifunctional Asphalt Mixtures. *Renew. Sustain. Energy Rev.* **2021**, *151*, 111552, doi:10.1016/j.rser.2021.111552.
2. Ibrahim, S.H.; Ibrahim, N.I.A.; Wahid, J.; Goh, N.A.; Koesmeri, D.R.A.; Nawi, M.N.M. The Impact of Road Pavement on Urban Heat Island (UHI) Phenomenon. *Int. J. Technol.* **2018**, *9*, 1597, doi:10.14716/ijtech.v9i8.2755.
3. Piracha, A.; Chaudhary, M.T. Urban Air Pollution, Urban Heat Island and Human Health: A Review of the Literature. *Sustainability* **2022**, *14*, 9234, doi:10.3390/su14159234.
4. Chen, G.; Chen, Y.; Tan, X.; Zhao, L.; Cai, Y.; Li, L. Assessing the Urban Heat Island Effect of Different Local Climate Zones in Guangzhou, China. *Build. Environ.* **2023**, *244*, 110770, doi:10.1016/j.buildenv.2023.110770.
5. Andrade, C.; Fonseca, A.; Santos, J.A. Climate Change Trends for the Urban Heat Island Intensities in Two Major Portuguese Cities. *Sustainability* **2023**, *15*, 3970, doi:10.3390/su15053970.
6. Vardhu, V.A.K.; Sharma, Dr.A. Classification, Mitigations and Methods to Detect UHI: A Review. *INTERANTIONAL J. Sci. Res. Eng. Manag.* **2023**, *07*, doi:10.55041/IJSREM17711.
7. Mondal, S. Phase Change Fibers. In *Handbook of Fibrous Materials*; Hu, J., Kumar, B., Lu, J., Eds.; Wiley, 2020; pp. 263–279 ISBN 978-3-527-34220-4.
8. Betancourt-Jimenez, D.; Montoya, M.; Haddock, J.; Youngblood, J.P.; Martinez, C.J. Regulating Asphalt Pavement Temperature Using Microencapsulated Phase Change Materials (PCMs). *Constr. Build. Mater.* **2022**, *350*, 128924, doi:10.1016/j.conbuildmat.2022.128924.
9. Chou, H.-M.; Chen, C.-R.; Nguyen, V.-L. A New Design of Metal-Sheet Cool Roof Using PCM. *Energy Build.* **2013**, *57*, 42–50, doi:10.1016/j.enbuild.2012.10.030.
10. Osterman, E.; Tyagi, V.V.; Butala, V.; Rahim, N.A.; Stritih, U. Review of PCM Based Cooling Technologies for Buildings. *Energy Build.* **2012**, *49*, 37–49, doi:10.1016/j.enbuild.2012.03.022.
11. Pinheiro, C.; Hammes, N.; Lima, O.; Landi, S.; Homem, N.; Rocha Segundo, I.; Felgueiras, H.P.; Freitas, E.; Costa, M.F.M.; Carneiro, J. Reducing the Effects of Low Albedo of Asphalt Materials Incorporating Polyethylene Glycol (PEG) 1000, 2000 and 4000 as Phase Change Materials (PCM). *EPJ Web Conf.* **2023**, *287*, 09024, doi:10.1051/epjconf/202328709024.

12. Pinheiro, C.; Landi, S.; Lima, O.; Ribas, L.; Hammes, N.; Segundo, I.R.; Homem, N.C.; Castelo Branco, V.; Freitas, E.; Costa, M.F.; et al. Advancements in Phase Change Materials in Asphalt Pavements for Mitigation of Urban Heat Island Effect: Bibliometric Analysis and Systematic Review. *Sensors* **2023**, *23*, 7741, doi:10.3390/s23187741.
13. Baetens, R.; Jelle, B.P.; Gustavsen, A. Phase Change Materials for Building Applications: A State-of-the-Art Review. *Energy Build.* **2010**, *42*, 1361–1368, doi:10.1016/j.enbuild.2010.03.026.
14. Diaconu, B.M.; Varga, S.; Oliveira, A.C. Experimental Assessment of Heat Storage Properties and Heat Transfer Characteristics of a Phase Change Material Slurry for Air Conditioning Applications. *Appl. Energy* **2010**, *87*, 620–628, doi:10.1016/j.apenergy.2009.05.002.
15. Gil, A.; Oró, E.; Peiró, G.; Álvarez, S.; Cabeza, L.F. Material Selection and Testing for Thermal Energy Storage in Solar Cooling. *Renew. Energy* **2013**, *57*, 366–371, doi:10.1016/j.renene.2013.02.008.
16. Yinfei, D.; Pusheng, L.; Jiacheng, W.; Hancheng, D.; Hao, W.; Yingtao, L. Effect of Lightweight Aggregate Gradation on Latent Heat Storage Capacity of Asphalt Mixture for Cooling Asphalt Pavement. *Constr. Build. Mater.* **2020**, *250*, 118849, doi:10.1016/j.conbuildmat.2020.118849.
17. Cunha, S.; Leite, P.; Aguiar, J. Characterization of Innovative Mortars with Direct Incorporation of Phase Change Materials. *J. Energy Storage* **2020**, *30*, 101439, doi:10.1016/j.est.2020.101439.
18. Kulkarni, P.; Muthadhi, A. Thermal Energy Storage Cement Mortar with Direct Incorporation of Organic and Inorganic Phase Change Materials. *Innov. Infrastruct. Solut.* **2021**, *6*, 30, doi:10.1007/s41062-020-00399-4.
19. Pérez-Silva, I.; Ibarra, I.S.; Castañeda-Ovando, A.; Galán-Vidal, C.A.; Páez-Hernández, Ma.E. Development of Cellulose Acetate Microcapsules with Cyanex 923 for Phenol Removal from Aqueous Media. *J. Chem.* **2018**, *2018*, 1–8, doi:10.1155/2018/9506489.
20. Gbekou, F.K.; Benzarti, K.; Boudenne, A.; Eddhahak, A.; Duc, M. Mechanical and Thermophysical Properties of Cement Mortars Including Bio-Based Microencapsulated Phase Change Materials. *Constr. Build. Mater.* **2022**, *352*, 129056, doi:10.1016/j.conbuildmat.2022.129056.
21. Drissi, S.; Ling, T.-C.; Mo, K.H. Development of Leak-Free Phase Change Material Aggregates. *Constr. Build. Mater.* **2020**, *230*, 117029, doi:10.1016/j.conbuildmat.2019.117029.
22. Rao, V.V.; Parameshwaran, R.; Ram, V.V. PCM-Mortar Based Construction Materials for Energy Efficient Buildings: A Review on Research Trends. *Energy Build.* **2018**, *158*, 95–122, doi:10.1016/j.enbuild.2017.09.098.
23. Abdullah, M.F.; Andriyana, A.; Muhamad, F.; Ang, B.C. Effect of Core-to-Shell Flowrate Ratio on Morphology, Crystallinity, Mechanical Properties and Wettability of Poly(Lactic Acid) Fibers Prepared via Modified Coaxial Electrospinning. *Polymer* **2021**, *237*, 124378, doi:10.1016/j.polymer.2021.124378.
24. Felgueiras, H.P.; Homem, N.C.; Teixeira, M.A.; Ribeiro, A.R.M.; Antunes, J.C.; Amorim, M.T.P. Physical, Thermal, and Antibacterial Effects of Active Essential Oils with Potential for Biomedical Applications Loaded onto Cellulose Acetate/Polycaprolactone Wet-Spun Microfibers. *Biomolecules* **2020**, *10*, 1129, doi:10.3390/biom10081129.
25. Ozipek, B.; Karakas, H. Wet Spinning of Synthetic Polymer Fibers. In *Advances in filament yarn spinning of textiles and polymers*; Elsevier, 2014; pp. 174–186.
26. Rohani Shirvan, A.; Nouri, A.; Sutti, A. A Perspective on the Wet Spinning Process and Its Advancements in Biomedical Sciences. *Eur. Polym. J.* **2022**, *181*, 111681, doi:10.1016/j.eurpolymj.2022.111681.
27. Tang, Z.; Jia, S.; Wang, F.; Bian, C.; Chen, Y.; Wang, Y.; Li, B. Highly Stretchable Core–Sheath Fibers via Wet-Spinning for Wearable Strain Sensors. *ACS Appl. Mater. Interfaces* **2018**, *10*, 6624–6635, doi:10.1021/acsami.7b18677.
28. Zhang, J.; Song, S.; Zhang, C.; Li, C.; Xu, J.; Xia, L.; Liu, X.; Xu, W. Fabrication of Leather-like Yarns Using Waste Leather for Textile Application. *Prog. Org. Coat.* **2024**, *186*, 108053, doi:10.1016/j.porgcoat.2023.108053.
29. Quan, Q.; Zhang, Y.; Piao, H.; Zhang, H.; Zhao, J. Polybutyrolactam (PBY) Fiber: A Promising Biobased and Biodegradable Fiber Fabricated by Dry-Jet-Wet Spinning. *Polymer* **2022**, *260*, 125392, doi:10.1016/j.polymer.2022.125392.
30. Teo, W.E.; Ramakrishna, S. A Review on Electrospinning Design and Nanofibre Assemblies. *Nanotechnology* **2006**, *17*, R89–R106, doi:10.1088/0957-4484/17/14/R01.
31. Zhang, W.; Zhang, X.; Xu, Y.; Xu, Y.; Qiao, J.; Shi, T.; Huang, Z.; Liu, Y.; Fang, M.; Min, X.; et al. Flexible Polyethylene Glycol/Polyvinylpyrrolidone Composite Phase Change Fibres: Preparation, Characterization, and Thermal Conductivity Enhancement. *Polymer* **2021**, *214*, 123258, doi:10.1016/j.polymer.2020.123258.
32. Mirabedini, A. *Developing Novel Spinning Methods to Fabricate Continuous Multifunctional Fibres for Bioapplications*; Springer Theses; Springer International Publishing: Cham, 2018; ISBN 978-3-319-95377-9.
33. Chen, C.; Zhao, Y.; Liu, W. Electrospun Polyethylene Glycol/Cellulose Acetate Phase Change Fibers with Core–Sheath Structure for Thermal Energy Storage. *Renew. Energy* **2013**, *60*, 222–225, doi:10.1016/j.renene.2013.05.020.
34. Swapnil, S.I.; Datta, N.; Mahmud, M.M.; Jahan, R.A.; Arafat, M.T. Morphology, Mechanical, and Physical Properties of Wet-spun Cellulose Acetate Fiber in Different Solvent-coagulant Systems and In-situ Crosslinked Environment. *J. Appl. Polym. Sci.* **2021**, *138*, 50358, doi:10.1002/app.50358.

35. Santos-Sauceda, I.; Castillo-Ortega, M.M.; Del Castillo-Castro, T.; Armenta-Villegas, L.; Ramírez-Bon, R. Electrospun Cellulose Acetate Fibers for the Photodecolorization of Methylene Blue Solutions under Natural Sunlight. *Polym. Bull.* **2021**, *78*, 4419–4438, doi:10.1007/s00289-020-03324-y.
36. Babapoor, A.; Karimi, G.; Golestaneh, S.I.; Mezjin, M.A. Coaxial Electro-Spun PEG/PA6 Composite Fibers: Fabrication and Characterization. *Appl. Therm. Eng.* **2017**, *118*, 398–407, doi:10.1016/j.applthermaleng.2017.02.119.
37. Homem, N.C.; Amorim, M.T.P. Synthesis of Cellulose Acetate Using as Raw Material Textile Wastes. *Mater. Today Proc.* **2020**, *31*, S315–S317, doi:10.1016/j.matpr.2020.01.494.
38. Puleo, A.C.; Paul, D.R.; Kelley, S.S. The Effect of Degree of Acetylation on Gas Sorption and Transport Behavior in Cellulose Acetate. *J. Membr. Sci.* **1989**, *47*, 301–332, doi:10.1016/S0376-7388(00)83083-5.
39. Homem, N.C.; Tavares, T.D.; Miranda, C.S.; Antunes, J.C.; Amorim, M.T.P.; Felgueiras, H.P. Functionalization of Crosslinked Sodium Alginate/Gelatin Wet-Spun Porous Fibers with Nisin Z for the Inhibition of Staphylococcus Aureus-Induced Infections. *Int. J. Mol. Sci.* **2021**, *22*, 1930, doi:10.3390/ijms22041930.
40. Kramar, A.; González-Benito, F.J. Cellulose-Based Nanofibers Processing Techniques and Methods Based on Bottom-Up Approach—A Review. *Polymers* **2022**, *14*, 286, doi:10.3390/polym14020286.
41. Liu, L.; Gong, D.; Bratasz, L.; Zhu, Z.; Wang, C. Degradation Markers and Plasticizer Loss of Cellulose Acetate Films during Ageing. *Polym. Degrad. Stab.* **2019**, *168*, 108952, doi:10.1016/j.polymdegradstab.2019.108952.
42. Ahn, Y.-H.; DeWitt, S.J.A.; McGuire, S.; Lively, R.P. Incorporation of Phase Change Materials into Fibers for Sustainable Thermal Energy Storage. *Ind. Eng. Chem. Res.* **2021**, *60*, 3374–3384, doi:10.1021/acs.iecr.0c06140.
43. Ibrahim, M.M.; Fahmy, T.Y.; Salaheldin, E.I.; Mobarak, F.; Youssef, M.A.; Mabrook, M.R. Role of Tosyl Cellulose Acetate as Potential Carrier for Controlled Drug Release. *Life Sci. J.* **2015**, *10*, 127–133.
44. Nikoomanesh, N.; Zandi, M.; Ganjloo, A. Development of Eco-Friendly Cellulose Acetate Films Incorporated with Burdock (Arctium Lappa L.) Root Extract. *Prog. Org. Coat.* **2024**, *186*, 108009, doi:10.1016/j.porgcoat.2023.108009.
45. Fei, P.; Liao, L.; Cheng, B.; Song, J. Quantitative Analysis of Cellulose Acetate with a High Degree of Substitution by FTIR and Its Application. *Anal. Methods* **2017**, *9*, 6194–6201, doi:10.1039/C7AY02165H.
46. Frisoni, G.; Baiardo, M.; Scandola, M.; Lednická, D.; Cnockaert, M.C.; Mergaert, J.; Swings, J. Natural Cellulose Fibers: Heterogeneous Acetylation Kinetics and Biodegradation Behavior. *Biomacromolecules* **2001**, *2*, 476–482, doi:10.1021/bm0056409.
47. Huda, E.; Rahmi; Khairan Preparation and Characterization of Cellulose Acetate from Cotton. *IOP Conf. Ser. Earth Environ. Sci.* **2019**, *364*, 012021, doi:10.1088/1755-1315/364/1/012021.
48. Zhuang, J.; Li, M.; Pu, Y.; Ragauskas, A.; Yoo, C. Observation of Potential Contaminants in Processed Biomass Using Fourier Transform Infrared Spectroscopy. *Appl. Sci.* **2020**, *10*, 4345, doi:10.3390/app10124345.
49. Zhu, Q.; Wu, H.; Ma, Z.; Liu, Y.; Li, J.; Zhu, L.; Zhang, X.; Wang, C.; Chen, D.; Zhu, D. Micro-Volume Blood Separation Membrane for In-Situ Biosensing. *Biosensors* **2022**, *12*, 712, doi:10.3390/bios12090712.
50. Quan, S.; Li, S.; Wang, Z.; Yan, X.; Guo, Z.; Shao, L. A Bio-Inspired CO ₂ -Philic Network Membrane for Enhanced Sustainable Gas Separation. *J. Mater. Chem. A* **2015**, *3*, 13758–13766, doi:10.1039/C5TA03232F.
51. Snyder, R.G.; Hsut, S.L.; Krimm, S. Vibrational Spectp in the C-H Stretching Region and the Structure of the Polymethylene Chain.
52. Hospodarova, V.; Singovszka, E.; Stevulova, N. Characterization of Cellulosic Fibers by FTIR Spectroscopy for Their Further Implementation to Building Materials. *Am. J. Anal. Chem.* **2018**, *09*, 303–310, doi:10.4236/ajac.2018.96023.
53. Das, A.M.; Ali, A.A.; Hazarika, M.P. Synthesis and Characterization of Cellulose Acetate from Rice Husk: Eco-Friendly Condition. *Carbohydr. Polym.* **2014**, *112*, 342–349, doi:10.1016/j.carbpol.2014.06.006.
54. Chen, J.; Xu, J.; Wang, K.; Cao, X.; Sun, R. Cellulose Acetate Fibers Prepared from Different Raw Materials with Rapid Synthesis Method. *Carbohydr. Polym.* **2016**, *137*, 685–692, doi:10.1016/j.carbpol.2015.11.034.
55. Lopes, S.; Bueno, L.; Aguiar Júnior, F.D.; Finkler, C. Preparation and Characterization of Alginate and Gelatin Microcapsules Containing Lactobacillus Rhamnosus. *An. Acad. Bras. Ciênc.* **2017**, *89*, 1601–1613, doi:10.1590/0001-3765201720170071.
56. Zhu, S.; Ji, T.; Niu, D.; Yang, Z. Investigation of PEG/Mixed Metal Oxides as a New Form-Stable Phase Change Material for Thermoregulation and Improved UV Ageing Resistance of Bitumen. *RSC Adv.* **2020**, *10*, 44903–44911, doi:10.1039/D0RA08398D.
57. Sundararajan, S.; Samui, A.B.; Kulkarni, P.S. Shape-Stabilized Poly(Ethylene Glycol) (PEG)-Cellulose Acetate Blend Preparation with Superior PEG Loading via Microwave-Assisted Blending. *Sol. Energy* **2017**, *144*, 32–39, doi:10.1016/j.solener.2016.12.056.

58. Faradilla, R.F.; Lee, G.; Sivakumar, P.; Stenzel, M.; Arcot, J. Effect of Polyethylene Glycol (PEG) Molecular Weight and Nanofillers on the Properties of Banana Pseudostem Nanocellulose Films. *Carbohydr. Polym.* **2019**, *205*, 330–339, doi:10.1016/j.carbpol.2018.10.049.
59. Shaikh, H.M.; Anis, A.; Poulose, A.M.; Al-Zahrani, S.M.; Madhar, N.A.; Alhamidi, A.; Aldeligan, S.H.; Alsubaie, F.S. Synthesis and Characterization of Cellulose Triacetate Obtained from Date Palm (Phoenix Dactylifera L.) Trunk Mesh-Derived Cellulose. *Molecules* **2022**, *27*, 1434, doi:10.3390/molecules27041434.
60. Ribeiro, S.D.; Meneguin, A.B.; Barud, H. da S.; Silva, J.M.; Oliveira, R.L.; Asunção, R.M.N. de; Tormin, T.F.; Muñoz, R.A.A.; Filho, G.R.; Ribeiro, C.A. Synthesis and Characterization of Cellulose Acetate from Cellophane Industry Residues. Application as Acetaminophen Controlled-Release Membranes. *J. Therm. Anal. Calorim.* **2022**, *147*, 7265–7275, doi:10.1007/s10973-021-11022-8.
61. Vinodhini, P.A.; K., S.; Thandapani, G.; P.N., S.; Jayachandran, V.; Sukumaran, A. FTIR, XRD and DSC Studies of Nanochitosan, Cellulose Acetate and Polyethylene Glycol Blend Ultrafiltration Membranes. *Int. J. Biol. Macromol.* **2017**, *104*, 1721–1729, doi:10.1016/j.ijbiomac.2017.03.122.
62. Ansu, A.K.; Pandya, M.; Sharma, R.K.; Tripathi, D. *Experimental Investigation of Hybrid PCM Polyethylene Glycol with Al 2 O 3 and CuO Nanoparticles*; In Review, 2022;
63. Chen, C.; Wang, L.; Huang, Y. Electrospun Phase Change Fibers Based on Polyethylene Glycol/Cellulose Acetate Blends. *Appl. Energy* **2011**, *88*, 3133–3139, doi:10.1016/j.apenergy.2011.02.026.
64. Cai, Y.; Gao, C.; Xu, X.; Fu, Z.; Fei, X.; Zhao, Y.; Chen, Q.; Liu, X.; Wei, Q.; He, G.; et al. Electrospun Ultrafine Composite Fibers Consisting of Lauric Acid and Polyamide 6 as Form-Stable Phase Change Materials for Storage and Retrieval of Solar Thermal Energy. *Sol. Energy Mater. Sol. Cells* **2012**, *103*, 53–61, doi:10.1016/j.solmat.2012.04.031.
65. Gonçalves, S.M.; Dos Santos, D.C.; Motta, J.F.G.; Santos, R.R.D.; Chávez, D.W.H.; Melo, N.R.D. Structure and Functional Properties of Cellulose Acetate Films Incorporated with Glycerol. *Carbohydr. Polym.* **2019**, *209*, 190–197, doi:10.1016/j.carbpol.2019.01.031.